# Viscosity, tribological and physicochemical features of ZnO and MoS2 diesel oil-based nanofluids: An experimental study

Seyed Borhan Mousavi, Saeed Zeinali Heris, Patrice Estellé

# Viscosity, tribological and physicochemical features of ZnO and $MoS_2$ diesel oil-based nanofluids: An experimental study

Seyed Borhan Mousavi[a], Saeed Zeinali Heris[a*], Patrice Estellé[b]

[a] Faculty of Chemical and Petroleum Engineering, University of Tabriz, Tabriz, Iran

[b] Univ Rennes, LGCGM, EA3913, F-35000 Rennes, France

*s.zeinali@tabrizu.ac.ir

**Abstract**

In this research, two different diesel oil-based nanofluids were prepared and the influence of temperature and nanoparticle content were examined on viscosity, tribological, and physicochemical features of diesel oil. The kinematic viscosity of samples was experimentally evaluated based on standard ASTM D445. The greatest viscosity increment was diagnosed at 0.7 wt.% and 100°C for both of the prepared nanofluids. The anti-friction behavior of the nanofluids was studied utilizing a pin-on-disc tribometer. The acquired outcomes revealed that ZnO and $MoS_2$ nanoparticles (NPs) could promote the tribological characteristics of pure diesel oil. By analyzing the friction coefficient values and line roughness of the wear surface (Ra), an optimal concentration of ZnO and $MoS_2$ nanoparticles (NPs) were found to be around 0.4 wt.% and 0.7 wt.%, respectively. The friction factor and pumping power were also measured at diverse content of nanoparticles and flow rates showing that the pumping power was enhanced by the incorporation of nanoparticles.

**Keywords**: Viscosity; Tribological behavior; Physicochemical characteristic; Nano-ZnO; Nano-$MoS_2$; Diesel oil-based nanofluid

## Nomenclature

| | | |
|---|---|---|
| A | Cross section area ($m^2$) |
| D | Pipe diameter (m) |
| f | Friction factor |
| Q | Flow rate ($m^3\ s^{-1}$) |
| t | Time (s) |
| u | Velocity ($m\ s^{-1}$) |
| V | Volume ($m^3$) |
| Re | Reynolds number |
| L | Length (m) |
| wt | Nanoparticle weight fraction (%) |
| m | Mass (kg) |
| T | Temperature (°C) |
| d | Diameter (m) |
| M | Molecular mass ($kg\ mol^{-1}$) |
| N | Avogadro number ($mol^{-1}$) |

## Greek letters

| | |
|---|---|
| $\nu$ | Kinematic viscosity ($mm^2\ s^{-1}$) |
| $\rho$ | Density ($kg\ m^{-3}$) |
| $\varphi$ | Volume fraction (%) |

## Subscripts

| | |
|---|---|
| th | Theoretical |
| exp | Experimental |
| bf | Base fluid |

nf Nanofluid

np Nanoparticle

## 1. Introduction

The term nanofluid refers to the stable distribution of low concentrations of nanoparticles (NPs) with sizes ranging from 1 to 100 nm in a liquid [1, 2]. Nanofluids have been widely used due to their greater thermal behaviors in comparison with the base fluid. Furthermore, having more substantial surface areas than micro-sized particles and letting more inconsiderable erosion in comparison with the traditional liquid-solid blends can be mentioned as the benefits of nanofluids [3-8]. This exceptional improvement in characteristics is associated with the size and shape of the NPs and their nature [9]. Several kinds of nanoparticles including metallic and nonmetallic, with various forms and dimensions, were utilized to prepare nanofluids, and some inspiring outcomes have been evidenced; however, the usage of nanoparticles may lead to accretion in viscosity of the nanofluids owing to their viscose nature [10-22]. Recently, ZnO NPs have attracted remarkable research attention owing to their capacity for advancing thermophysical qualities, tribological properties, and good dispersion traits [23-29]. $MoS_2$ NPs have exhibited excellent anti-wear, mechanical, and thermophysical properties among various types of nanoparticles. Their lubricity characteristics associate with the inherent structure namely the vast space and weak Van der Waals forces that lead them to move easily on each other [30-32].

Numerous comparisons have been performed to examine the anti-wear features and thermal performances of nano-$MoS_2$ additive oil-based fluids. The outcomes confirmed that the tribological and thermal aspects of the prepared nanofluids are strikingly enhanced by adding nano-$MoS_2$ particles to the utilized fluid [30, 33-35]. Dinesh et al. [36] scrutinized the tribological and thermophysical characteristics of engine oil comprising MWCNT and Zinc Oxide NPs. The outcomes demonstrated that MWCNT and Zinc Oxide NPs were able to advance the operational facets of the engine oil. Esfe et al. [37] analyzed the rheological attributes of engine oil utilizing MWCNT and ZnO NPs. The conclusions showed that the usability of the nano-additives in the engine oil can decrease the damages to motor sections in a cold start of the vehicle. The tribological properties of different base oils using ZnO and CuO NPs as additives have been studied by Alves et al [38]. They reported that by adding nanoparticles to conventional oil, the anti-frictional features could be remarkably enhanced. A

more constant tribo-film had made on the worn surface, which was adequate for the further decreased friction. Cabaleiro et al. [39] assessed the thermal features of multiple $TiO_2$ nanofluids. They observed that the prepared nanofluids increased thermal conductivity in comparison with pure fluids. Probes of the lubricating, rheological, and thermal performances of ZnO NPs demonstrated that adding nano zinc oxide particles to the pure fluid can develop the mentioned traits [40-46]. Hu et al. [47] conducted a tribological comparison between three different types of $MoS_2$ in various greases. The results explicated that any $MoS_2$ enhanced the wear resistance of the three greases in most cases under the chosen measurement conditions. Zawawi et al. [48, 49] studied thermal conductivity and viscosity behaviors of three diverse mixtures of nanoparticles in the base lubricant (PAG composite nano-lubricants) at diverse nanoparticle volume levels and temperatures. They found that the usage of nanoparticles in the pure lubricant improved the thermophysical traits such as thermal conductivity and dynamic viscosity. Coelho et al. [50] analyzed the thermophysical qualities of CuO nanofluids. The results declared that both permittivity and electrical conductivity developed with the addition of nano-CuO particles. Ding et al. [51] conducted a study for understanding the tribological features of silica NPs water-based lubricants. They published that the silica NPs can significantly improve the tribological performances when added to the base lubricant. Empirical research of the thermal characteristics of $Al_2O_3$/water nanofluid proved that adding $Al_2O_3$ NPs as an additive can substantially raise the thermal traits of the nanofluid [52-56]. Karimi et al. [57] estimated the thermal conductivity acts of $NiFe_2O_4$ nanofluids at diverse concentrations. They noticed that the thermal conductivity of the samples raised with the increasing temperature and content. Minea et al. [58] conducted a study to compare the thermophysical qualities of diverse nanofluids. The outcomes manifested that adding alumina to the ionic liquid can exceptionally enhance thermophysical properties. Research performed by Zhengfeng et al. [59] proved that the addition of three kinds of nano-montmorillonite as additives in the grease can enhance the lubricity attributes. Lou et al. [60] researched to examine the lubricity aspects of the $Al_2O_3$ oil-based nano-lubricants. The outcomes exposed that adding nano-$Al_2O_3$ particles to the pure oil can notably enhance tribological properties; moreover, the pure oil containing 0.1 wt.% nano-$Al_2O_3$ particles had the lowest friction coefficient. Grecov et al. [61-66] investigated the effect of cellulose and liquid crystals as an additive on the tribological and rheological properties of both aqueous-based and oil-based lubricants. The results proved that the used additives had great

potential in friction reduction applications. Wu et al. [67] prepared $MoS_2$ nanosheets decorated by zinc borate (ZB) NPs and applied them as additives to assess the anti-frictional behavior of lubricating oil, confirming that they can dramatically advance the tribological characteristics. Sanukrishna et al. [68] examined the impressions of nano-$TiO_2$ particles (0.07~0.8% volume fractions) on rheological properties and thermal conductivity on PAG nano-lubricant at diverse temperatures, showing that the utilized nanoparticles can develop the examined properties. Sharif et al. [69] studied thermophysical behaviors of the $Al_2O_3$/polyalkylene glycol nano-lubricants at different content of additives and temperatures exhibiting that the measured quantities enhanced with utilizing the additives. Khairul et al. [70] studied the stability and thermal characteristics of different prepared nanofluids. They showed that the efficiency of the system developed with the usage of the nanoparticles. Jabbari et al. [71] reviewed the thermophysical qualities of various nanofluids, confirmed that the thermophysical attributes of nanofluids increased with raising nanoparticle volume fraction.

According to the conducted literature review, the preponderance of examinations in the aforementioned area announces a positive impact on the rheological, anti-friction, and thermal features of different types of additives. Based on the investigations in the field of nanofluids, comprehensive examinations have been carried out on nanofluids namely turbine meter oil, engine oil, grease, water-based nanofluids, and other nanofluids, while limited consideration has been paid to the area of diesel oil. Consequently, in this article, the impact of ZnO and $MoS_2$ NPs on viscosity, tribological, and physicochemical qualities were studied. It is worth stating that this work is a continuation of the previous one [72] to complete the characterization and demonstrate the potential of nano-lubricants considering different measurements.

In the current investigation, diesel oil-based nanofluids were prepared using a two-step preparation technique with 0.1, 0.4, and 0.7 wt.% of ZnO and $MoS_2$ NPs, and the impact of nanoparticle concentration on the viscosity, tribological, and physicochemical features of the nanofluids was analyzed.

## 2. Experimental materials and methods

### 2.1 Materials

Zinc oxide (ZnO) and molybdenum disulfide ($MoS_2$) as the precursor, SAE-40 monograde diesel engine oil as the core fluid, and Triton X-100 as the surfactant were procured from US

Research-Nanomaterials, Sigma-Aldrich, Pars oil co, and Samchun, respectively. Table 1 presents the main features of the nanoparticles from the manufacturer data. Characteristics of the base fluid are shown in Table 2. SEM characterization (Zeiss, Germany) was performed for the analysis of ZnO and $MoS_2$ NPs. The crystalline form of the used nanoparticles was examined using powder X-ray diffraction (XRD, PHILIPS-PW1730, Netherlands) with Cu-K$\alpha$ radiation ($\lambda$ = 0.14056 nm) at room temperature. The XRD patterns were performed at room temperature ranging in $2\theta = 7 - 80°$ at a rate of 3° $min^{-1}$. The Debye–Scherrer's formula was applied to compute the crystallite size of the nanoparticles, based on the XRD schema [73]:

$$D = \frac{0.9*\lambda}{\beta(cos\theta)} \quad (1)$$

Where $D$, $\lambda$, $\beta$, and $\theta$ are the particle size perpendicular to the regular line of plane, the wavelength of X-ray, the entire width at the half summit of the diffraction peak, and the Bragg angle of the peak.

**Table 1** Properties of the nanoparticles.

| **Properties** | ZnO | $MoS_2$ |
|---|---|---|
| **Color** | White | Gray/Black |
| **Purity (%)** | 99.9 | 99 |
| **Density (g/cm$^3$)** | 5.6 | 5.06 |
| **Size (nm)** | 30 | 90 |

**Table 2** Characteristics of the diesel oil.

| **Base Fluid** | **Physical properties** | **Value** |
|---|---|---|
| Monograde diesel oil (SAE-40) | **Pour point**, **°C** | -17.8 |
| | **Flash point**, **°C** | 238 |
| | **Density**, **Kg/cm$^3$ at 15 °C** | 0.893 |
| | **Kinematic viscosity**, **cSt at 40 °C** | 162.53 |
| | **Kinematic viscosity**, **cSt at 100 °C** | 14.62 |
| | **Viscosity Index (VI)** | 86.85 |

## 2.2 Preparation of nanofluids

The nano-ZnO and nano-$MoS_2$ particles were added to the diesel oil at 0.1, 0.4, and 0.7 wt.%. The nanofluids were prepared at different concentrations from 0.02 wt.% to 0.8 wt.%; however, there were no conspicuous differences between the results for each test at the concentration below the 0.1 wt.%. The most significant reason for this phenomenon is the fact that because of the high viscosity of the base diesel oil, nanoparticles could not strikingly affect the investigated parameters at lower concentrations—that is— below the 0.1 wt.%. To possess satisfying dispersibility, Triton X-100 (mass proportion of 1 to 2 with nanoparticle) as the surfactant was poured into the nanofluid mixture. The required value of nanoparticles and surfactant were accurately balanced employing a precision electronic balance and mixed with the diesel oil. The suspension was mixed using a mechanical stirrer at 900 rpm for about 3 hours and was agitated with an ultrasonic agitator (Parsonic 2600s, Iran) for about 45 min to provide a stable nanofluid. The sonication operated at a frequency of 28 kHz and a nominal power of 70 W at room temperature. Multiple concentrations were prepared to study the influence of the nanoparticle content.

## 2.3 Kinematic viscosity analysis

The kinematic viscosity was assessed based on ASTM D445. The kinematic viscosity was assessed using an Opaque viscometer (Accuracy: $\pm$0.3%) at atmospheric pressure. The viscometer bath was employed to control the temperature. All analyses were conducted three times. Kinematic viscosity of the prepared nanofluids was discovered at 40°C – 100°C.

## 2.4 Tribological analysis

The tribological features of the produced nanofluids at various concentrations were assessed and compared to the base diesel oil using a pin-on-disc tribometer based on the ASTM G99. The tribological experiments were carried out at 25℃ with a sliding velocity of 150 rpm and a weight of 75 N. The analyses were carried out under various loading bars varying from 20 N to 75 N; however, because of the high viscosity of diesel oil, lower loading bars could not affect, and significant change was not seen in the recorder COF values. Thus, 75 N was considered as the loading bar. The sliding length was 1000 m. The material of the pins was hardened bearing steel (AISI 52100). The diameter and length of the pins were 5 mm and 50 mm, respectively. Before the tribological examination, the pin and disc were purified utilizing acetone. The normal force was applied applying load rings. The specimen is rotated at a selected speed. The rotation of the

sample and the sample holder were controlled by the motor. The examinations were done using the prepared nanofluids, and outcomes were compared with the pure diesel fluid. The friction coefficient values were reported; furthermore, the surface roughness $R_a$ was measured. All tests were replicated at least three times, and the average value of each was determined.

### 2.5 Friction factor determination

The friction factor and the pressure drop of nano-lubricants in a copper tube were measured using an experimental setup described as follows. The system consisted of a pump to transport the working fluids at different velocities, a fluid tank, valves, pressure gauges, and a flow meter. Fig. 1 exhibits the schematic of the system.

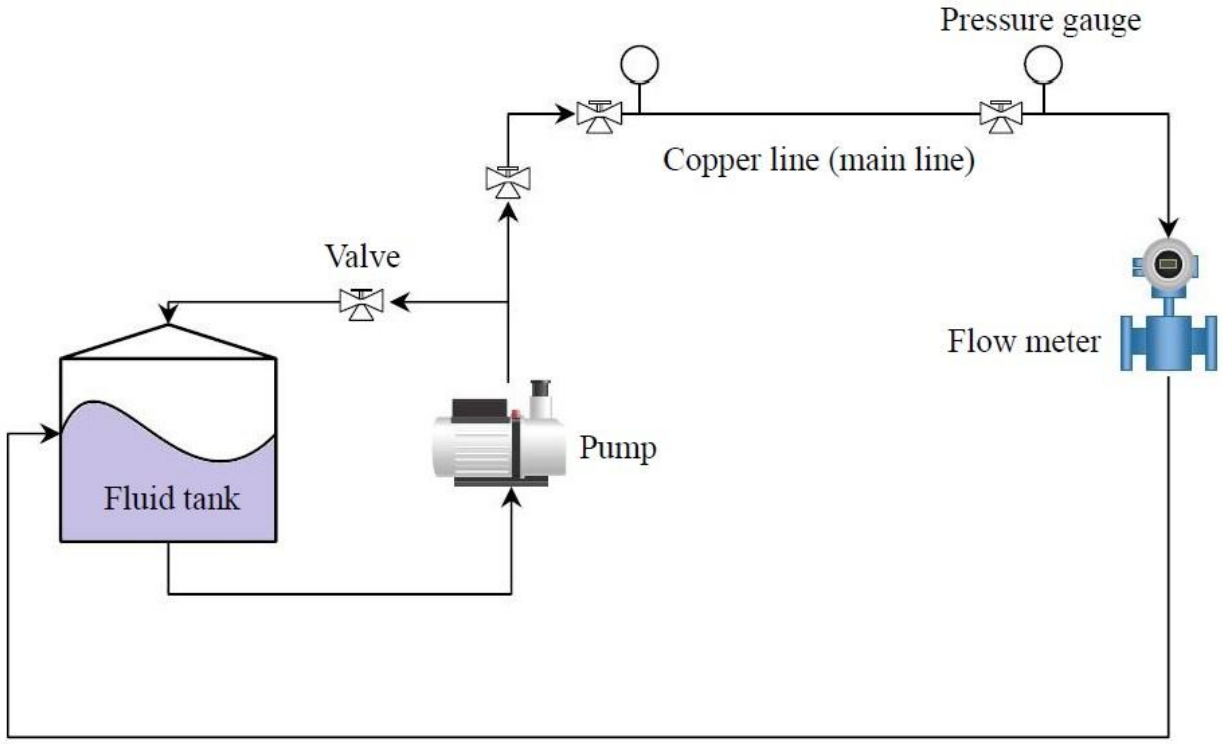


**Fig. 1.** Design of the laboratory device.

## 3. Data and uncertainty analysis

The theoretical friction factor (f) for laminar flow and Reynolds number are obtained as [74, 75]:

$$f = \frac{64}{Re} \quad (2)$$

$$Re = \frac{uD}{\nu} \quad (3)$$

where $D$, $u$, $\nu$ and are the diameter of the pipe as a specific length, velocity, and kinematic viscosity, and $Re$ is Reynolds number. Velocity and flow rate circumscribed by Eqs. (4) and (5), sequentially [76].

$$u = \frac{Q}{A} \quad (4)$$

$$Q = \frac{V}{t} \quad (5)$$

where $t$, $V$, $A$, $Q$ and are time, volume, the cross-section area of the pipe, and flow rate.

Theoretical ($\Delta P_{th}$) pressure difference was defined by Eq. (6) [77].

$$\Delta P_{th} = f\frac{L}{D} * \frac{\rho u^2}{2} \quad (6)$$

$L$ and $\rho$ are the pipe length and density of the fluid.

The pumping power was determined by utilizing Eq. (7).

$$W = Q\Delta P_{exp} \quad (7)$$

Considering the devices employed in this research have various precision and the parameters were estimated with these tools possess errors, it is essential to examine the impact of analysis error on these outcomes. If P is a function of empirical variables such as $x_1$, $x_2$, $x_3$, …, $x_n$, the subsequent formula is applied to assess the determination error of the parameter $x_i$ [78]:

$$U_{P_i} = \frac{x_i}{P}\frac{\partial P}{\partial x_i}u_{x_i} \quad (8)$$

where $x_i$ is the assessable quantity and $u_{x_i}$ is the determination error. The highest error of parameter P is determined by merging the error of per parameter $x_i$ utilizing the subsequent formula:

$$U_P = \pm\left\{\left(\frac{x_1}{P}\frac{\partial P}{\partial X x_1}U u_{x_1}\right)^2 + \left(\frac{x_2}{P}\frac{\partial P}{\partial x_2}u_{x_2}\right)^2 + \cdots + \left(\frac{x_n}{P}\frac{\partial P}{\partial x_n}u_{x_n}\right)^2\right\}^{1/2} \quad (9)$$

As stated earlier, the Reynolds number is determined as $Re = \frac{uD}{\nu}$, and the generated error from the Reynolds number is proved as follows:

$$U_{Re} = \sqrt{(U_u)^2 + (U_D)^2 + (-U_\nu)^2} \quad (10)$$

Given that $u = \frac{Q}{A}$, $U_U$ is computed as follows:

$$U_U = \sqrt{\left(U_Q\right)^2 + (-U_A)^2} \quad (11)$$

Additionally, the generated error by the volumetric flow rate is determined as $Q = \frac{V}{t}$ that is defined by Eq. (12).

$$U_Q = \sqrt{(U_V)^2 + (-U_t)^2} \quad (12)$$

The error of the friction factor ascertainment is similar to the error correlated with the Reynolds number.

$$U_f = U_{Re} \quad (13)$$

Hence, the highest friction factor error in the analyses reached 1.1%.

Errors for all measured parameters are calculated as follows:

The mass of base fluid: $U_{m_{bf}} = \pm\frac{0.001}{98.6} = \pm 1.014 \times 10^{-5}$

The mass of nanoparticle: $U_{m_{np}} = \pm\frac{0.001}{0.2} = \pm 5 \times 10^{-3}$

The nanoparticle weight fraction: $U_{wt} = \pm[{U_{m_{bf}}}^2 + {U_{m_{np}}}^2]^{1/2} = \pm 5 \times 10^{-3}$

The temperature: $U_T = \pm\frac{0.02}{40} = \pm 5 \times 10^{-4}$

The kinematic viscosity: $U_\nu = \pm\frac{0.02}{40} = \pm 5 \times 10^{-4}$

## 4. Results and discussion

### 4.1 Materials: characterization

The SEM pictures of the nano-ZnO and nano-$MoS_2$ particles are displayed in Fig. 2. Based on the SEM pictures, the nano-ZnO and nano-$MoS_2$ particles have a nearly spherical form and platelet-like shape with an average diameter of 30 nm and 90 nm, respectively. The XRD

patterns of the nano-ZnO and nano-$MoS_2$ particles are displayed in Fig. 3. The XRD pattern of the ZnO NPs shows peaks at $2\theta$ = 31.88, 34.58, 36.43, 47.73, 56.73, 62.93, 66.83, 68.03, and 69.13, which can be classified to the (100), (002), (101), (102), (110), (103), (200), (112) and (201) planes of ZnO. All diffraction peaks were in arrangement with the diffraction data of the standard card (JCPDS card number 36-1451) [79]. The XRD pattern of the $MoS_2$ NPs displays diffraction peaks at $2\theta$ = 14.63, 29.18, 32.88, 39.73, 44.38, 50.13, 60.48 and 70.23 matching to the (002), (004), (100), (103), (104), (105), (112), and (200) crystal planes of the $MoS_2$ structure according to the source data of JCPDS card number 37-1492 [80]. No impurity peaks were identified. The crystallite sizes of ZnO and $MoS_2$ calculated according to the principal peak breadth in the XRD schema by Eq. (1) were 14.2 nm and 32.6 nm, respectively. The nanoparticles are presented with an agglomeration of several crystals; thus, in most cases, the average diameter of nanoparticles is higher than the crystallite size. Comparing the average diameter and crystallite size of nanoparticles, it can be concluded that ZnO NPs are more agglomerated.

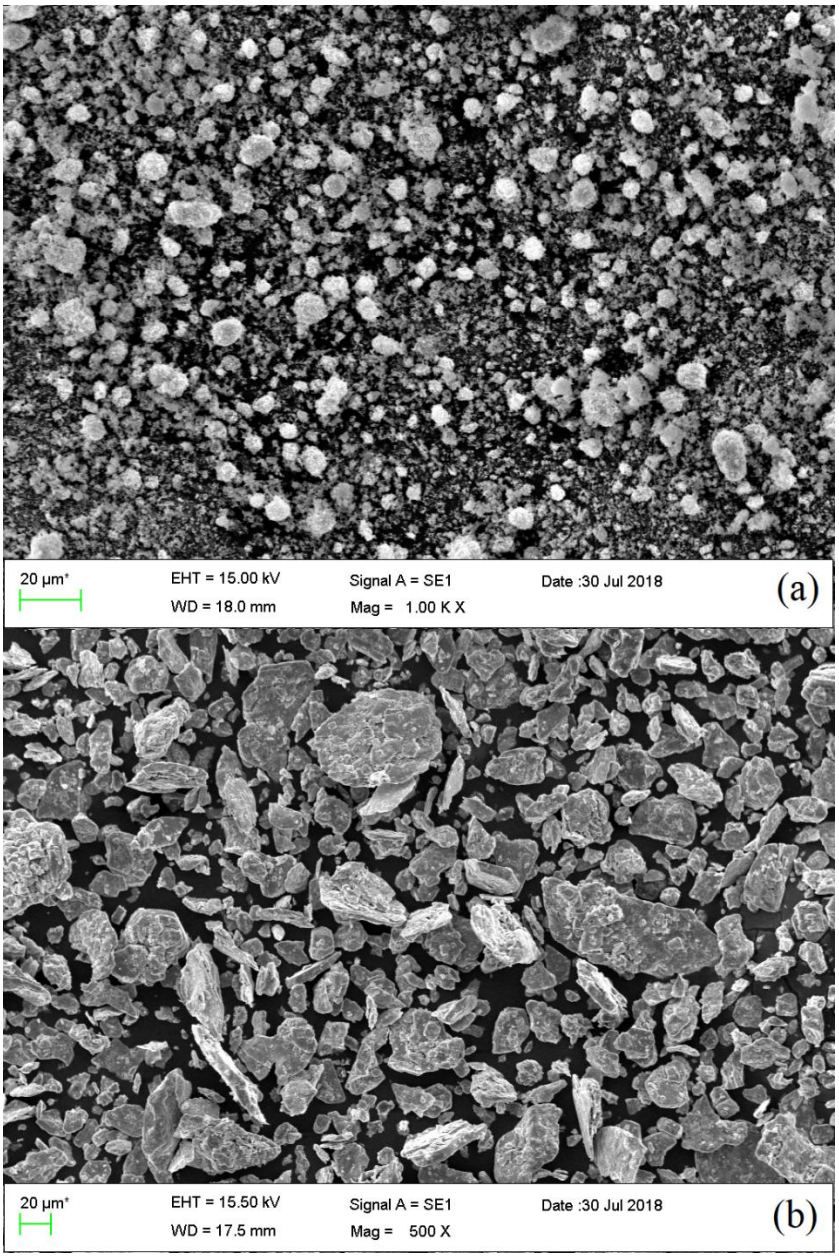


**Fig. 2.** SEM images of (a) ZnO NPs, (b) $MoS_2$ NPs.

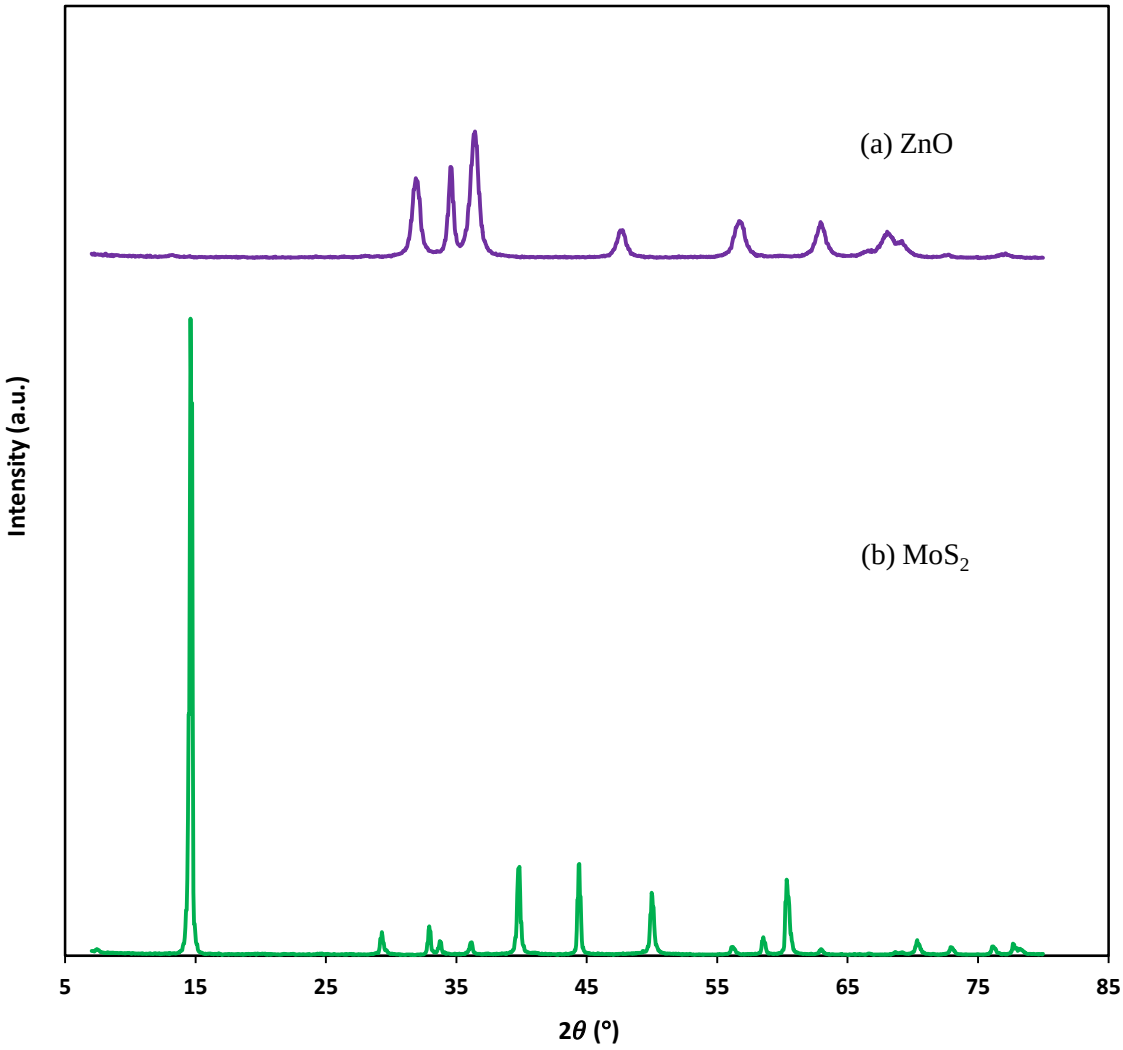


**Fig. 3.** XRD patterns of (a) ZnO NPs, (b) $MoS_2$ NPs.

### 4.2 Viscosity

Fig. 4. depicts the impact of the ZnO and $MoS_2$ NPs concentration and temperature on the kinematic viscosity of the diesel oil, at 40°C – 100°C. According to Fig. 4, it can be seen that the kinematic viscosity of all specimens including ZnO and $MoS_2$ NPs, has increased concerning the pure diesel oil. The increase was more substantial at greater concentrations because of the agglomeration of the increase in nanoparticles. While the temperature rises, the kinematic viscosity of all specimens was reduced since the intermolecular strengths are weakened by increasing the temperature. At each measured temperature, ZnO nanofluids showed higher viscosity values than diesel oil comprising nano-$MoS_2$ particles since the ZnO nanofluids are

more stable and the nano-ZnO particles are more coherent compared to the $MoS_2$ nanofluids. The maximum viscosity increment was obtained at 0.7 wt.% and 100 °C for both prepared nanofluids. Considering the results, it can be concluded that the ZnO nanofluids were more resistant to move in comparison with the $MoS_2$ diesel oil-based nanofluids.

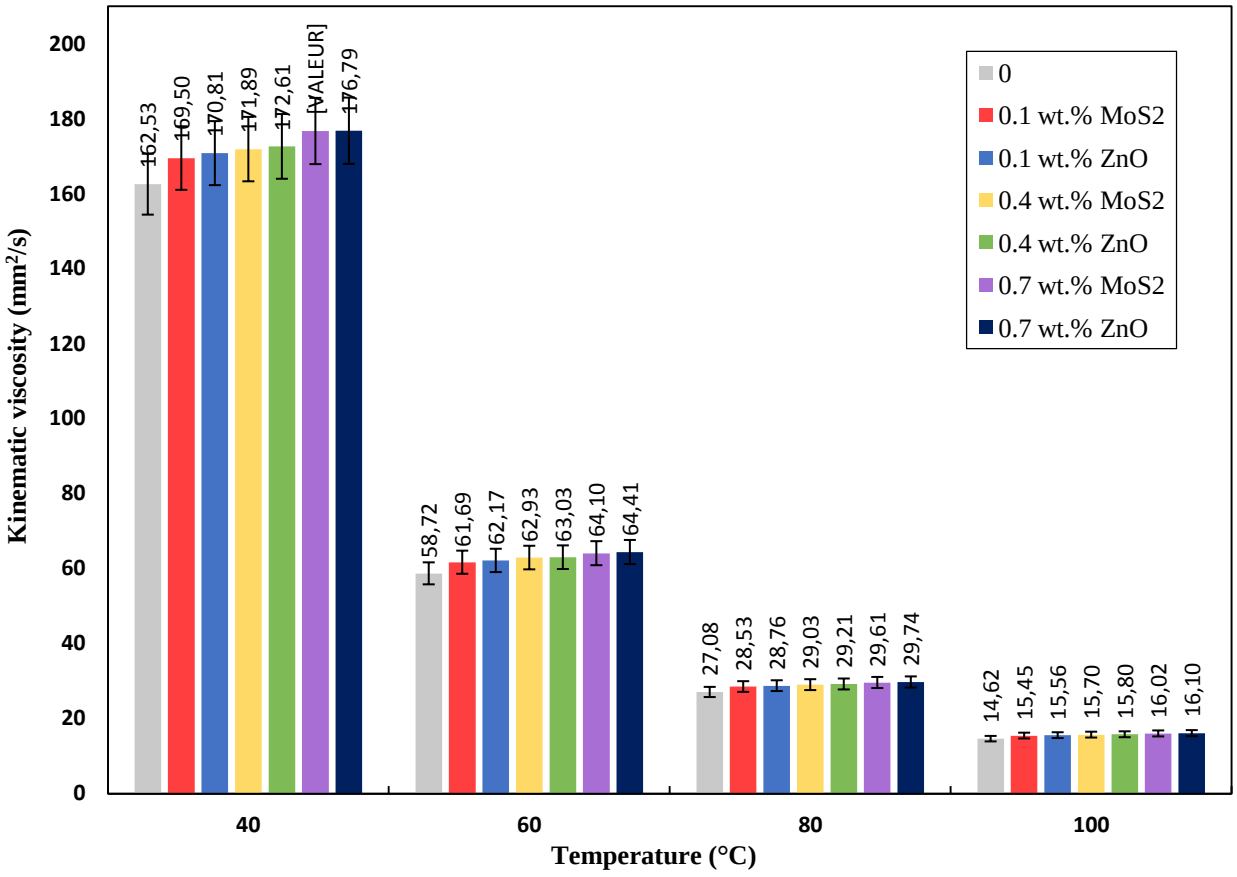


**Fig. 4.** Variation of kinematic viscosity of diesel oil containing ZnO and $MoS_2$ NPs at different concentrations with temperature.

One of the commonly utilized formulas for evaluating the relation between the viscosity and temperature of the manufacturing oils is Walther function, which is characterized by Eq. (14) [81]:

$$W = log(log(\nu + \varepsilon)) = b - n\,log\,T \quad (14)$$

Where $\nu$, $\varepsilon$, and $T$ are the kinematic viscosity ($mm^2/s$), 0.7 for the kinematic viscosity greater than 2 $mm^2/s$, the temperature (K), and $b$ and $n$ attribute to fixed parameters that are specified

based on the oil sort. The parameters b and n obtained from Eq. (14) for different concentrations of the ZnO and $MoS_2$ NPs are gathered in Table 3. According to the $R^2$ values, it can be asserted that the aforementioned model can properly determine the changes in the kinematic viscosity of the ZnO and $MoS_2$ NPs with temperature in the studied range.

**Table 3** Parameters acquired from the fitting of alteration in kinematic viscosity with temperature using the Walther function.

| Concentration (wt.%) | b | n | $R^2$ |
|---|---|---|---|
| 0 | 9.23 | 3.56 | 0.99 |
| 0.1 ZnO | 9.07 | 3.49 | 0.99 |
| 0.4 ZnO | 9.02 | 3.47 | 0.99 |
| 0.7 ZnO | 8.99 | 3.46 | 0.99 |
| 0.1 $MoS_2$ | 9.08 | 3.50 | 0.99 |
| 0.4 $MoS_2$ | 9.04 | 3.48 | 0.99 |
| 0.7 $MoS_2$ | 9.02 | 3.47 | 0.99 |

Einstein proposed the dependency of viscosity on the volume portion of the nanoparticles. Einstein assumed that the particles were in very dilute suspensions, namely solid spheres without interactions, and the improvement in the shear makes the rotary movement of the particles; thus, raises the dispersal viscosity. The Einstein formula, which can be utilized for suspensions having a particle volume portion below 0.01 ($\varphi < 0.02$) is depicted as follows [82]:

$$\eta_{nf} = \eta_{bf}(1 + 2.5\varphi) \quad (15)$$

$$\varphi = \frac{\left(\frac{m}{\rho}\right)_{np}}{\left(\frac{m}{\rho}\right)_{np} + \left(\frac{m}{\rho}\right)_{bf}} \quad (16)$$

where $\eta$, $\varphi$, $m$, and, $\rho$ are viscosity, the volume fraction of nanoparticles, mass, and density.

Many equations have been proposed to calculate the relative viscosity ($\eta_r = \frac{\eta_{nf}}{\eta_{bf}}$) using the volume portion of nanoparticles which are noted in Table 4. In equations, the diameter of the molecule of base fluid ($d_f$) was defined by Eq. (17).

$$d_f = 0.1\left(\frac{6M}{N\rho_f}\right)^{1/3} \quad (17)$$

Where $M$, $N$, and $\rho_f$ are the molecular mass of the diesel oil, Avogadro number, and the mass density of diesel oil calculated at temperature $T_0 = 293$ K. $d_p$ is the diameter of the nanoparticles.

The calculated values of the relative viscosity applying various models at different volume fractions of $MoS_2$ nanofluids are listed in Table 5. The alteration of the relative viscosity for $MoS_2$ nanofluids using different models and also the comparison between these models with the experimental data are presented in Fig. 5. As can be noticed in these figures, the theoretical models could not foretell the relative viscosity-mass fraction of the nanoparticles relation since these models did not ponder the size, shape, sort of the nanoparticles, sort of base fluids, and agglomeration of the nanoparticles, as well as temperature, while above-mentioned factors have a significant impression on the viscosity of nanofluids. As it is shown, the Einstein model unpredicted viscosity and this model was only developed for sphere nanoparticles. Numerous studies have also asserted similar conclusions considering different nanofluids, in which empirical results are not agreeable with the considered models [83-86].

**Table 4** Classic equations to calculate the relative viscosity.

| Author | Equation |
|---|---|
| Corcione [87] | $\frac{\eta_{nf}}{\eta_{bf}} = \frac{1}{1-34.87\left(\frac{d_p}{d_f}\right)^{-0.3}\varphi^{1.03}}$ |
| Sharma [88] | $\frac{\eta_{nf}}{\eta_{bf}} = \left(1+\frac{\varphi}{100}\right)^{11.3}\left(1+\frac{T_{nf}}{70}\right)^{-0.038}\left(1+\frac{d_p}{170}\right)^{-0.061}$ |

**Table 5** Relative viscosity of $MoS_2$ nanofluids at diverse volume fractions.

| Nanoparticle | | $MoS_2$ | | |
|---|---|---|---|---|
| Weight fraction (wt.%) | | 0.1 | 0.4 | 0.7 |
| Volume fraction ($\varphi$%) | | 0.018 | 0.071 | 0.126 |
| Relative viscosity | Einstein | 1.00045 | 1.00178 | 1.00315 |
| | Corcione | 1.00034 | 1.00138 | 1.0025 |
| | Sharma | 0.98299 | 0.98305 | 0.98311 |

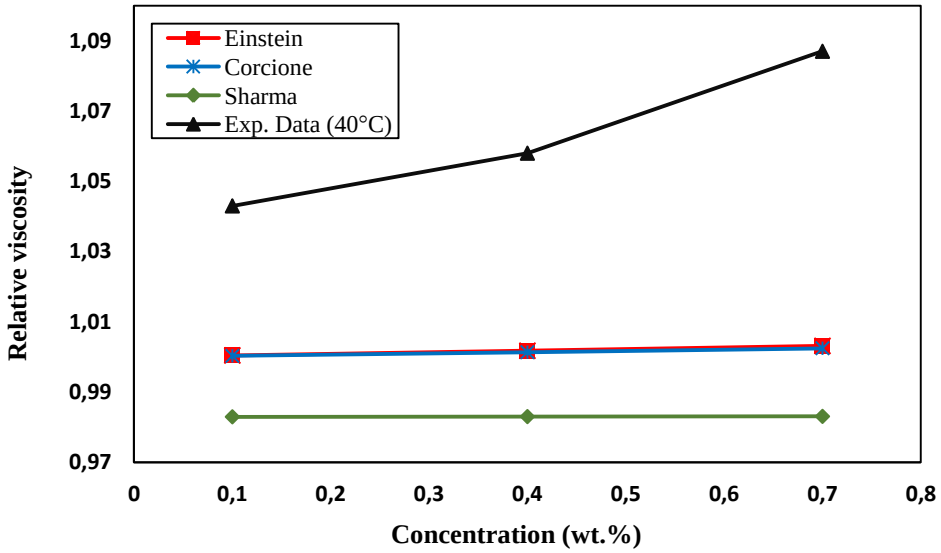


**Fig. 5.** Relative viscosity as a function of volume fraction for $MoS_2$ nanofluids.

### 4.3 Friction characteristics

Figs. 6 and 7 illustrate the recorded friction coefficients (COFs) vs time for the base sample, ZnO, and $MoS_2$ diesel oil-based nanofluids with various contents (0.1 ~ 0.7 wt.%) at rotating speed of 150 rpm and applied load of 75 N. The mean values of the COFs are also shown in Fig. 8. The performance of diesel oil without and with nanoparticles was assessed. The outcomes reveal that all the samples lead to an initial short running-in period and the COF stabilizes almost 300 seconds after the starting of the tribological analysis. Other researchers [89-91] also noticed similar conclusions concerning different nanofluids proving that the continuance of the run-in phase is reliant on various factors of the contact surfaces such as geometrical, chemical, and physical; moreover, the capacity of the lubricating fluid to produce a proper tribo-film. It is

determined that the average COFs of the nanofluids diminished with the content ranging from 0.1 wt.% to 0.7 wt.%. Fig. 6 shows that the friction coefficient diminished when the content of nano-ZnO particles was under 0.4 wt.%. However, when the content exceeded 0.4 wt.%, the friction coefficient increased. On the other hand, Fig. 7 shows that the friction coefficient values decreased by adding $MoS_2$ NPs. Based on Figs 6, 7, and 8, it can be understood that the COF values steadily decreased for $MoS_2$ nanofluids while for the ZnO nanofluids decreased first and then, gradually increased. Considering Fig. 8, it can be concluded that $MoS_2$ diesel oil-based nanofluids had a better anti-friction behavior compared to the ZnO nanofluids both in lower concentrations and higher concentrations. The lowest final COF in this research happened at a concentration of 0.7 wt.% $MoS_2$ nanofluids and the optimal content for ZnO NPs was 0.4 wt.%. Shape, size, morphology, and the inherent attributes of the nanoparticles play a vital role to develop the lubrication qualities of the nanofluids. Nanoparticles with lower diameter act better in anti-friction purposes in comparison with the greater ones in diameter. Nonetheless, in this investigation, the most influential factor in enhancing the lubricity performance of the $MoS_2$ nanofluids is the intrinsic structural features of the nano-$MoS_2$ particles which lead them to move easily on each other. Thus, the layers are located unitedly with low molecular forces and can readily move over each other.

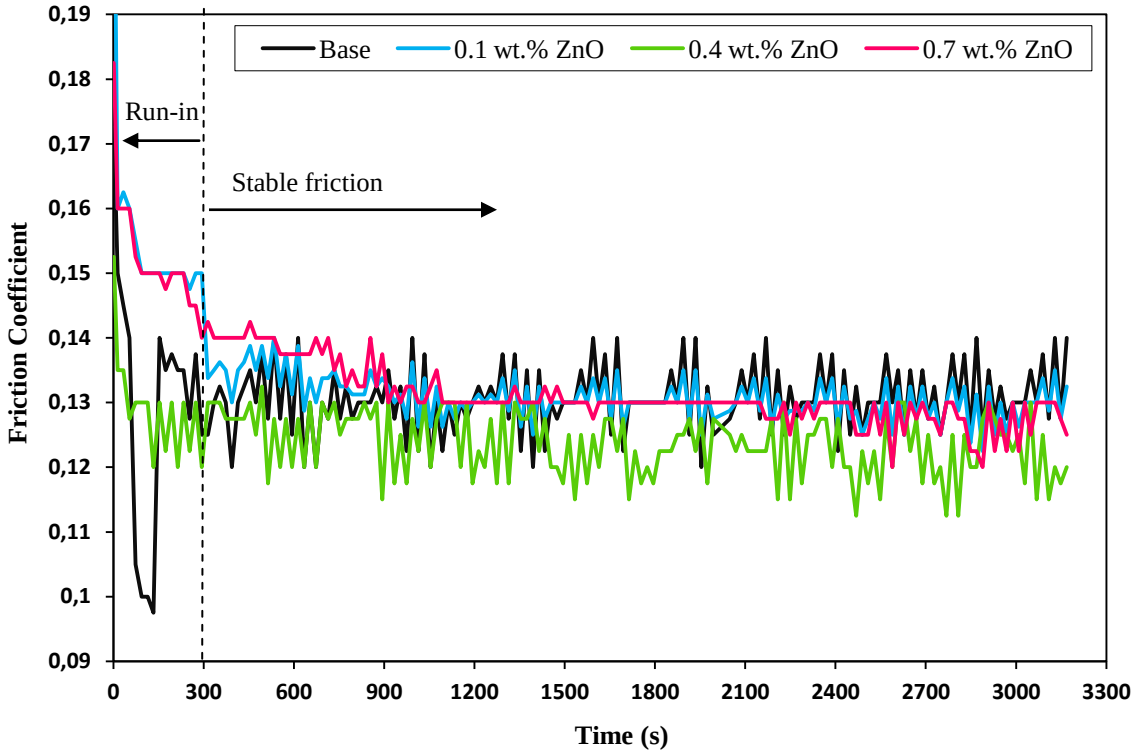


**Fig. 6.** Friction coefficient (COF) of the ZnO nanofluids with various contents as a function of time.

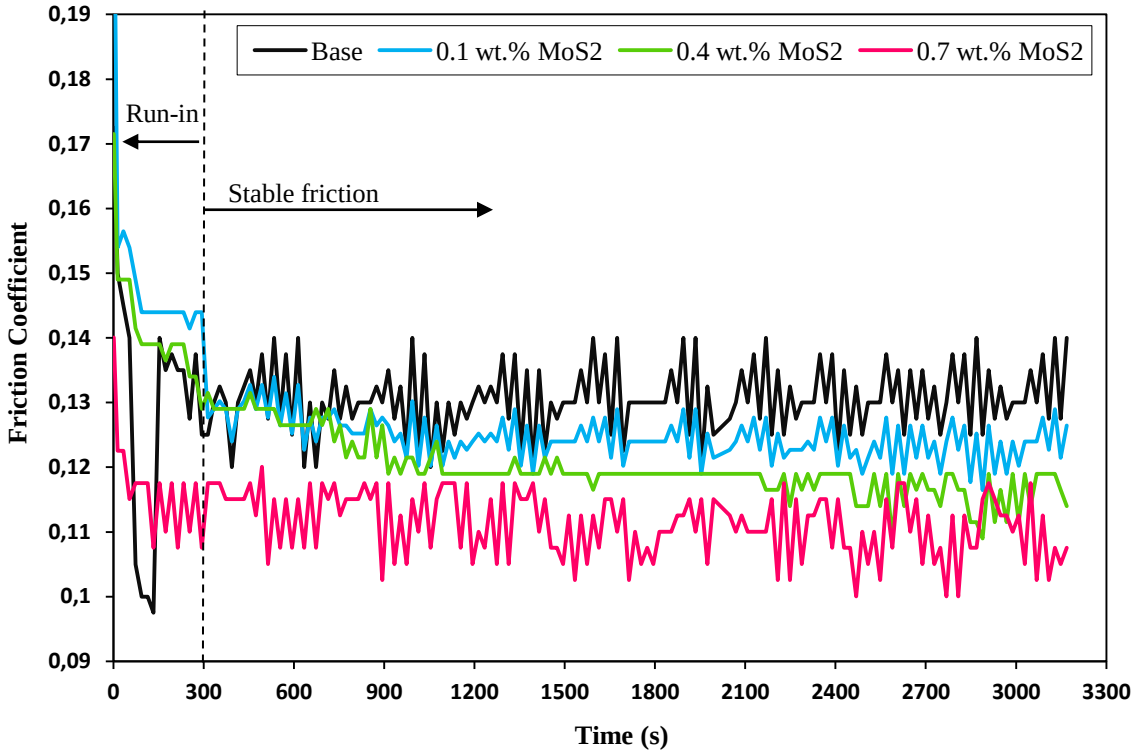


**Fig. 7.** Friction coefficient (COF) of the $MoS_2$ nanofluids with various contents as a function of time.

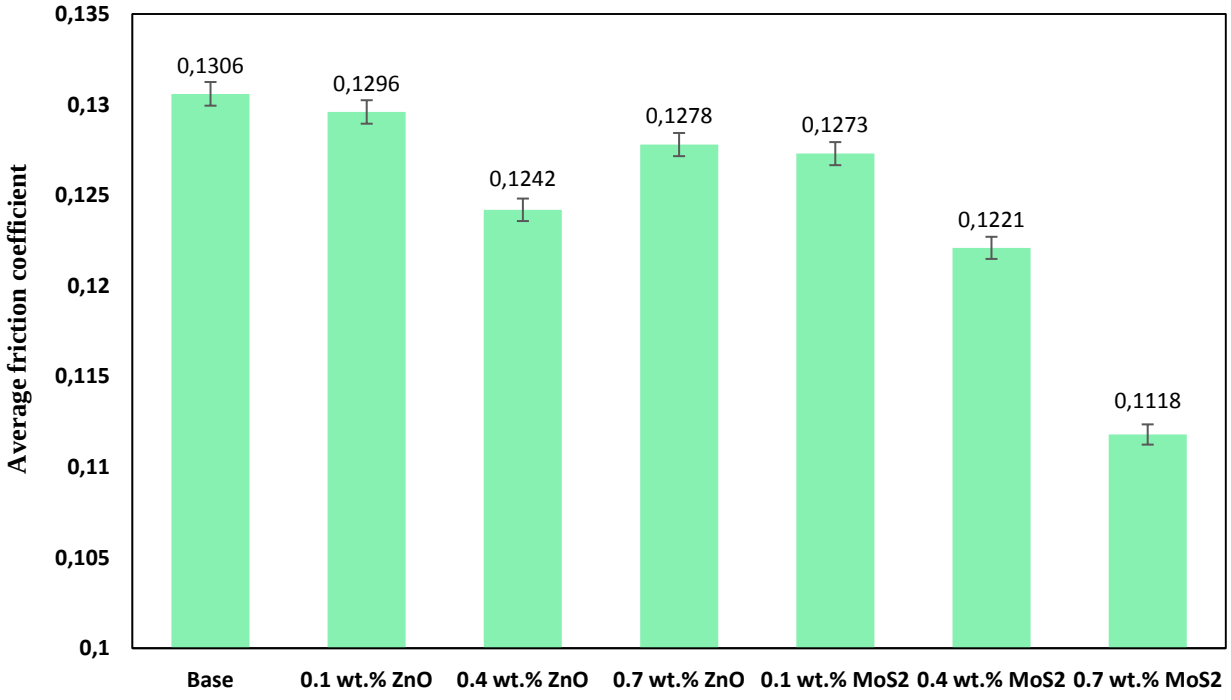


**Fig. 8.** Average friction coefficient (COF) values of the nanofluids at various concentrations.

Fig. 9 presents the characterizations of the wear mark on the rubbing superficies equal to the sliding path. The assessed line roughness $R_a$ values of the worn surfaces before and after the test at varying contents of ZnO and $MoS_2$ nanofluids are tabulated in Table 6. Based on the computed surface roughness ($R_a$), it can be discerned that the worn surfaces became smooth after the friction experiment due to the polishing impact of the diesel oil. Moreover, the roughness average of surfaces ($R_a$) decreased with the addition of the nanoparticles to the diesel oil. Having considered the pure diesel oil, the reduction of the $R_a$ values after the test was 3.64%, 21.33%, and 11.14% for 0.1 wt.%, 0.4 wt.%, and 0.7 wt.% ZnO nanofluids, respectively. Whereas the reduction of the $R_a$ values was 12.82%, 43.95%, and 60.75% for 0.1 wt.%, 0.4 wt.%, and 0.7 wt.% $MoS_2$ nanofluids. Hence, $MoS_2$ nanofluids showed lower $R_a$ values compared to those of ZnO nanofluids proving better anti-friction behavior of the $MoS_2$ NPs.

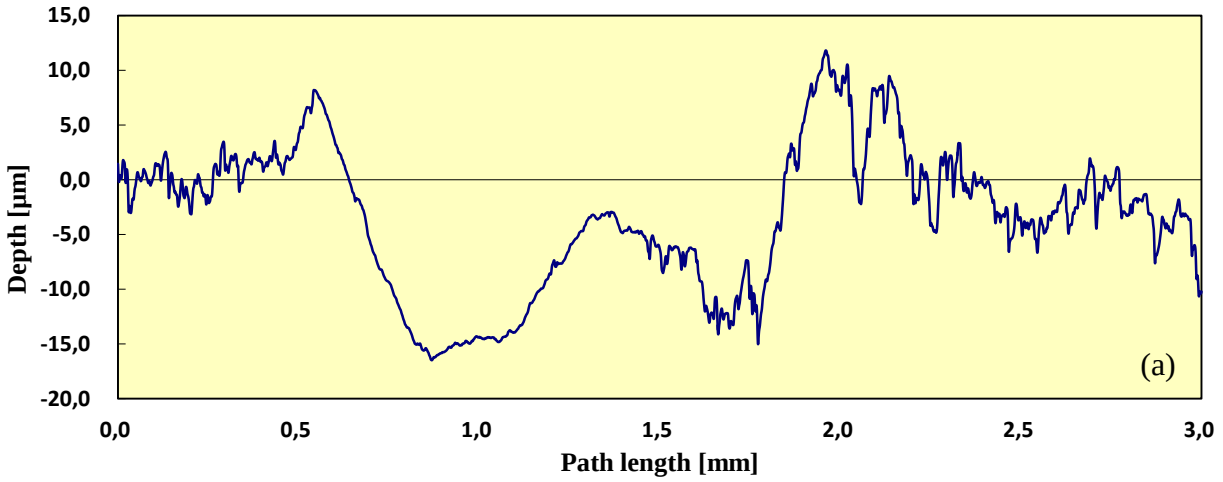


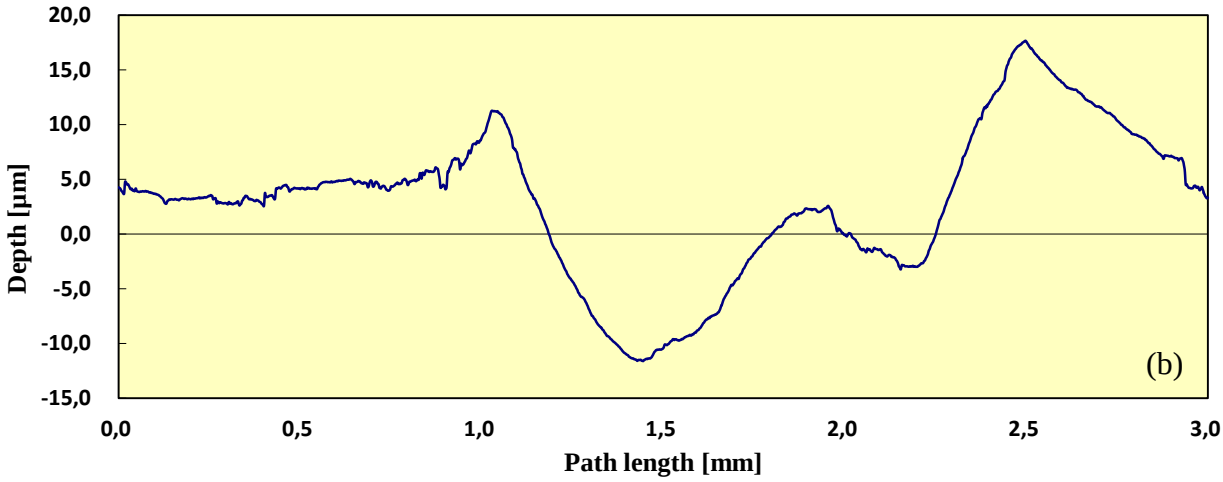

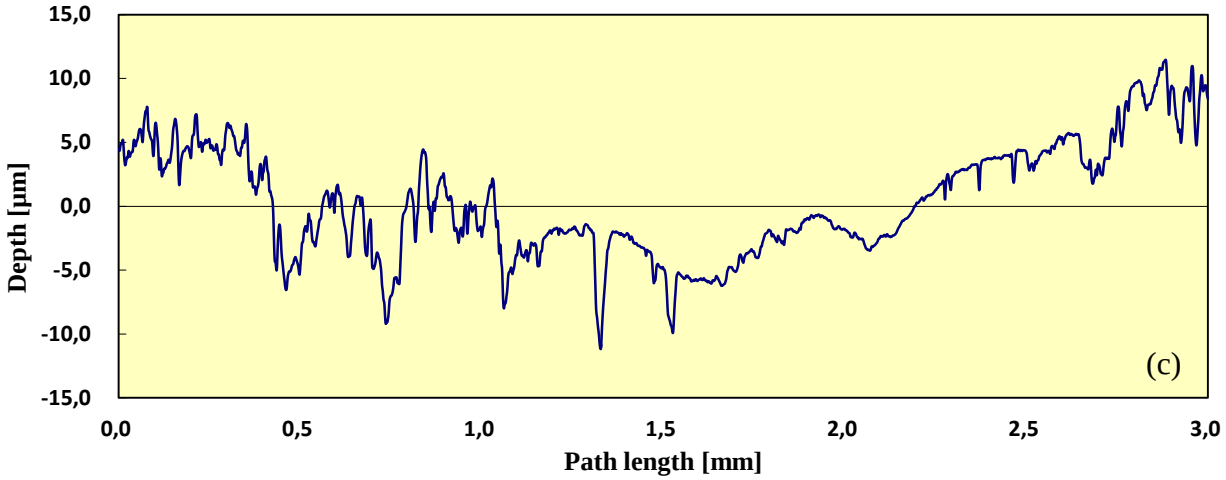
15,0
10,0
5,0
0,0
-5,0
-10,0
-15,0
Depth [µm]
0,0
0,5
1,0
1,5
2,0
2,5
3,0
Path length [mm]
(c)

1

2

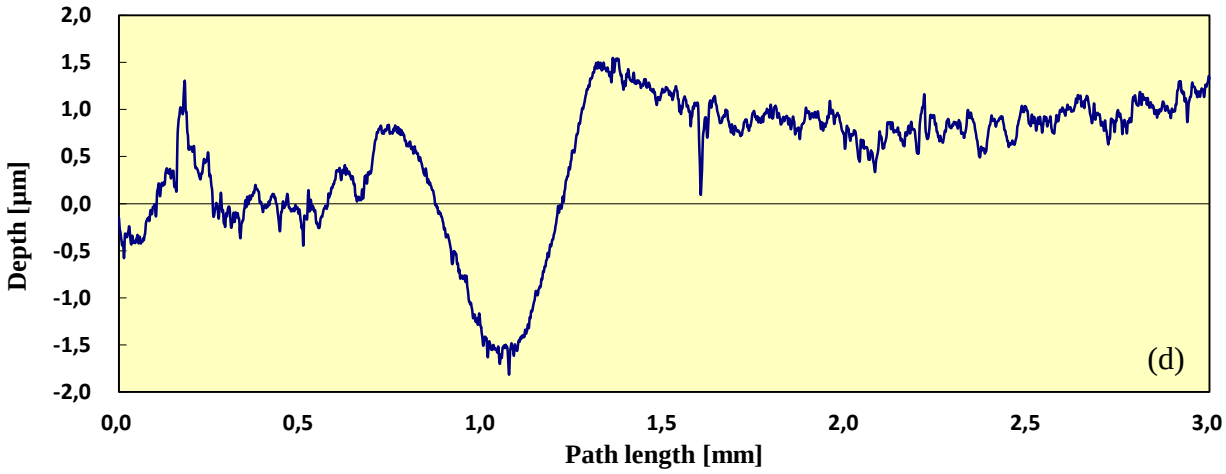
2,0
1,5
1,0
0,5
0,0
-0,5
-1,0
-1,5
-2,0
Depth [µm]
0,0
0,5
1,0
1,5
2,0
2,5
3,0
Path length [mm]
(d)

3

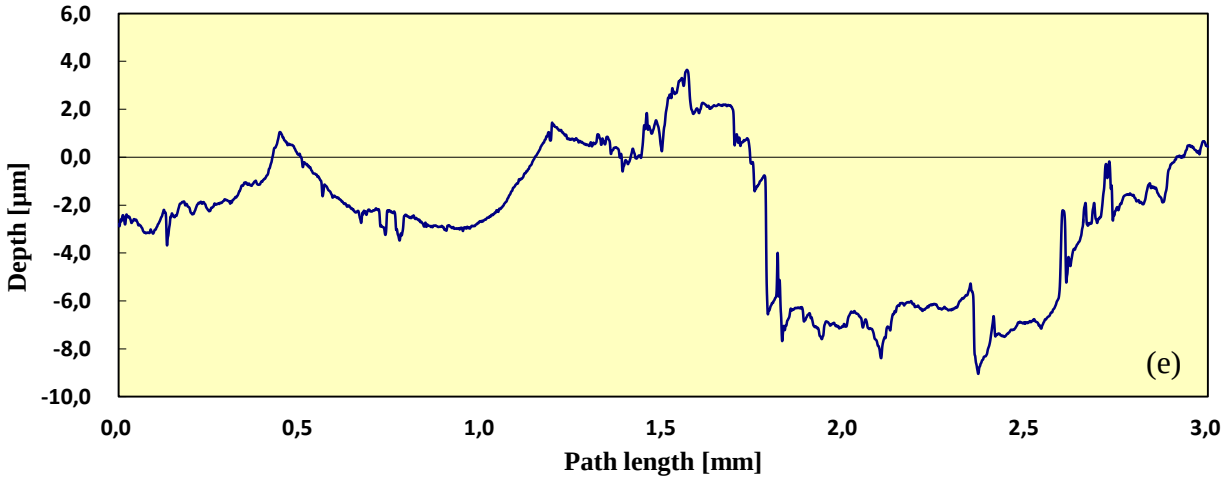
6,0
4,0
2,0
0,0
-2,0
-4,0
-6,0
-8,0
-10,0
Depth [µm]
0,0
0,5
1,0
1,5
2,0
2,5
3,0
Path length [mm]
(e)

4

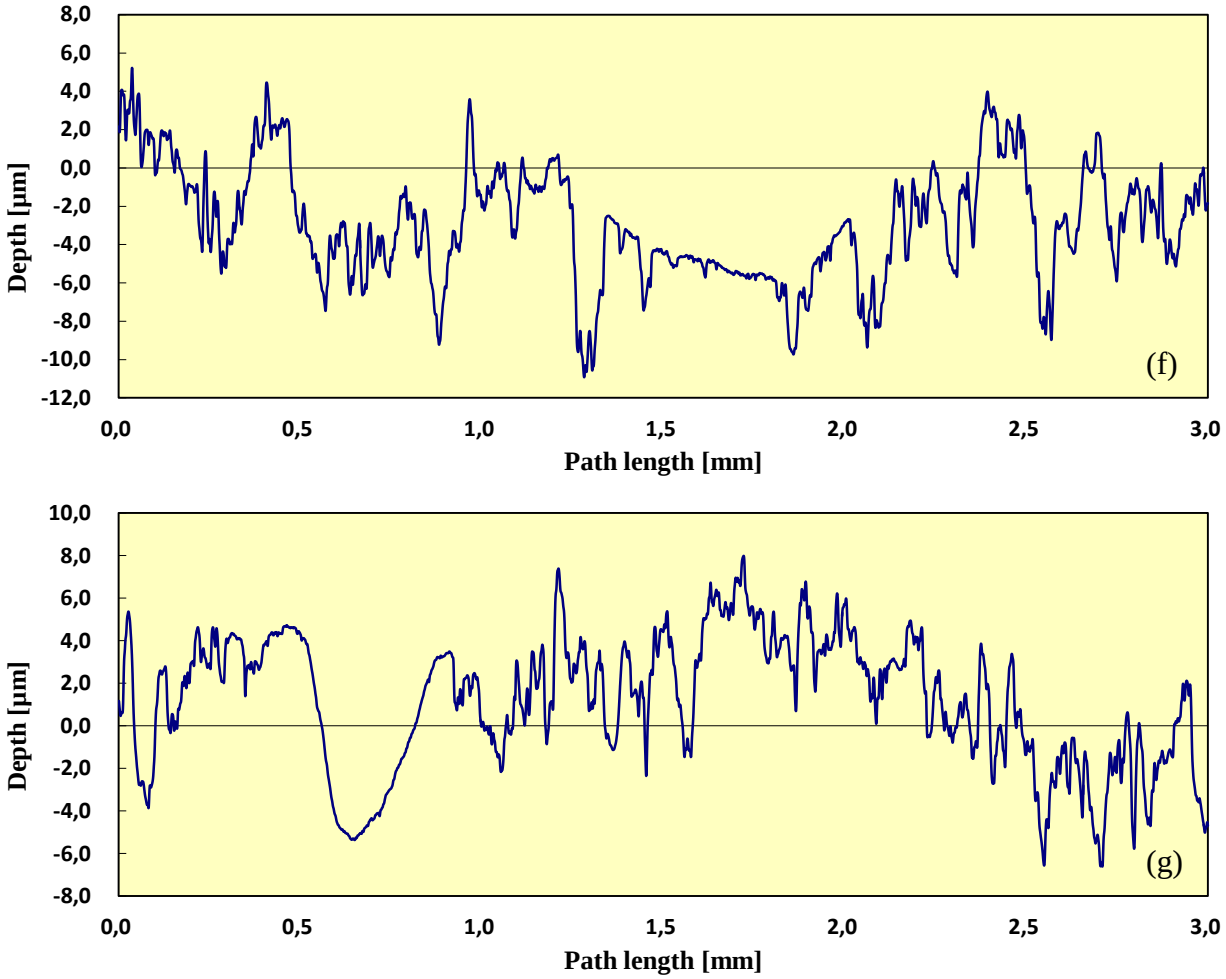


**Fig. 9.** Profile curve of wear scar of (a) pure diesel oil, (b) 0.1 wt.% ZnO nanofluids, (c) 0.4 wt.% ZnO nanofluids, (d) 0.7 wt.% ZnO nanofluids, (e) 0.1 wt.% $MoS_2$ nanofluids, (f) 0.4 wt.% $MoS_2$ nanofluids, (g) 0.7 wt.% $MoS_2$ nanofluids.

**Table 6** The measured surface roughness ($R_a$) values of the worn surfaces before and after the test at different concentrations of ZnO and $MoS_2$ nanofluids.

| Concentration (wt.%) | $R_a$ (before test)/μm | $R_a$ (after test)/μm | $\Delta R_a$/μm |
|---|---|---|---|
| 0 (pure diesel oil) | 6.922 | 5.136 | 1.786 |
| 0.1 ZnO | 6.971 | 5.120 | 1.851 |
| 0.4 ZnO | 5.942 | 3.775 | 2.167 |
| 0.7 ZnO | 6.395 | 4.410 | 1.985 |
| 0.1 $MoS_2$ | 4.601 | 2.586 | 2.015 |
| 0.4 $MoS_2$ | 5.016 | 2.445 | 2.571 |
| 0.7 $MoS_2$ | 5.279 | 2.413 | 2.866 |

### 4.4 Friction factor

The friction factor and the experimental pressure difference values were acquired using the devised laboratory at diverse flow rates for different nanofluids and the results were compared to the pure diesel oil. The variety of the friction factor at the measured flow rates, inlet velocity, Reynolds number, kinematic viscosity, the difference between the experimental and theoretical pressures at various content of nanoparticles are listed in Table 7. According to the data listed in Table 7, it can be concluded that the friction factor and Reynolds number had an opposite relation since the kinematic viscosity of the samples was increased by adding the nano-additives. At each flow rate, higher amounts of the friction factor were seen in comparison with the base fluid without nano-additives because by increasing the content of the nanoparticles, the kinematic viscosity of the nanofluids increased. By comparing the experimental and theoretical pressure values, it can be concluded that the laboratory had a proper performance. Based on the acquired outcomes, the pressure drops in the tube increased with the rising in the Reynolds number or inlet velocity. Recently, researchers have stated the identical trend for other nanofluids [31, 92]. The friction factor was raised in all contents of ZnO and $MoS_2$ NPs with the highest increment of 8.2 % and 8.3% for ZnO and $MoS_2$ nanofluids happening at 0.7 wt.% with the lowest inlet velocity.

**Table 7** The difference of friction factor at diverse flow rates for different nanofluids.

| Concentration (wt.%) | $Q \times 10^5$ ($m^3/s$) | $u$ (m/s) | $Re$ | $\nu \times 10^6$ ($m^2/s$) | $f$ | $\Delta P_{th}$ | $\Delta P_{exp}$ | Disparity (%) |
|---|---|---|---|---|---|---|---|---|
| 0 (pure diesel oil) | 1.022 | 0.161 | 6.18 | 234.065 | 10.36 | 14654.91 | 14130 | 3.58 |
| | 1.211 | 0.190 | 8.82 | 194.273 | 7.26 | 14302.62 | 13680 | 4.35 |
| | 3.614 | 0.568 | 29.67 | 172.341 | 2.16 | 38029.63 | 36150 | 4.94 |
| | 5.311 | 0.835 | 43.59 | 172.341 | 1.47 | 55932.20 | 52900 | 5.42 |
| 0.1 ZnO | 1.022 | 0.161 | 5.90 | 245.058 | 10.84 | 15331.46 | 14980 | 2.29 |
| | 1.211 | 0.190 | 8.41 | 203.804 | 7.61 | 14989.75 | 14250 | 4.94 |
| | 3.614 | 0.568 | 28.24 | 181.016 | 2.27 | 39959.97 | 38710 | 3.13 |
| | 5.311 | 0.835 | 41.50 | 181.016 | 1.54 | 58586.32 | 55400 | 5.44 |
| 0.4 ZnO | 1.022 | 0.161 | 5.85 | 247.333 | 10.95 | 15479.58 | 14600 | 5.68 |
| | 1.211 | 0.190 | 8.32 | 205.830 | 7.69 | 15140.03 | 14520 | 4.10 |
| | 3.614 | 0.568 | 27.96 | 182.889 | 2.29 | 40292.60 | 38350 | 4.82 |
| | 5.311 | 0.835 | 41.08 | 182.889 | 1.56 | 59318.58 | 57880 | 2.43 |
| 0.7 ZnO | 1.022 | 0.161 | 5.71 | 253.322 | 11.21 | 15839.33 | 14830 | 6.37 |
| | 1.211 | 0.190 | 8.13 | 210.767 | 7.87 | 15486.79 | 14450 | 6.69 |
| | 3.614 | 0.568 | 27.31 | 187.248 | 2.34 | 41152.09 | 36505 | 11.29 |
| | 5.311 | 0.835 | 40.12 | 187.248 | 1.60 | 60809.62 | 57540 | 5.38 |
| 0.1 $MoS_2$ | 1.022 | 0.161 | 5.95 | 243.190 | 10.76 | 15218.06 | 14725 | 3.24 |
| | 1.211 | 0.190 | 8.47 | 202.245 | 7.56 | 14891.01 | 14100 | 5.31 |
| | 3.614 | 0.568 | 28.46 | 179.629 | 2.25 | 39607.22 | 37970 | 4.13 |
| | 5.311 | 0.835 | 41.83 | 179.629 | 1.53 | 58204.90 | 56980 | 2.10 |
| 0.4 $MoS_2$ | 1.022 | 0.161 | 5.87 | 246.436 | 10.91 | 15421.96 | 14750 | 4.36 |
| | 1.211 | 0.190 | 8.36 | 205.024 | 7.66 | 15079.92 | 14265 | 5.40 |
| | 3.614 | 0.568 | 28.07 | 182.141 | 2.28 | 40113.88 | 38985 | 2.81 |
| | 5.311 | 0.835 | 41.25 | 182.141 | 1.55 | 58934.26 | 57655 | 2.17 |
| 0.7 $MoS_2$ | 1.022 | 0.161 | 5.70 | 253.585 | 11.22 | 15851.55 | 15150 | 4.43 |
| | 1.211 | 0.190 | 8.12 | 210.872 | 7.88 | 15504.60 | 15110 | 2.55 |
| | 3.614 | 0.568 | 27.30 | 187.278 | 2.34 | 41147.15 | 39880 | 3.08 |
| | 5.311 | 0.835 | 40.12 | 187.278 | 1.60 | 60802.32 | 58600 | 3.62 |

Fig. 10 exhibits the change of pumping power based on flow rates at various contents. Considering Fig. 10, it can be comprehended that the pumping power was enhanced by adding the nano-additives to the base fluid, as expected. The reason for this phenomenon is the fact that the pressure drops increased by increasing the flow rate, hence the increment in the pressure drop caused an augmentation in pumping power.

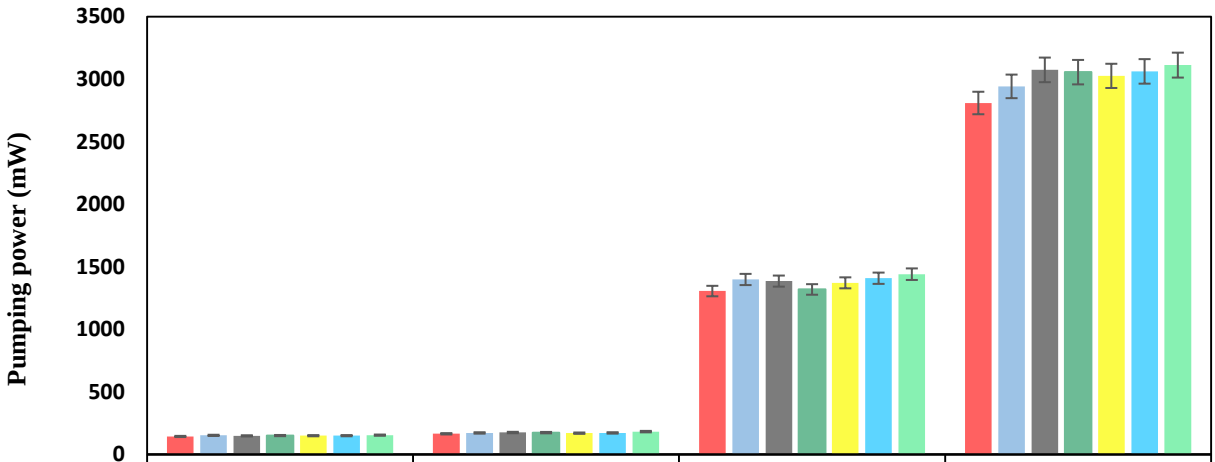


| | 1,02E-05 | 1,21E-05 | 3,61E-05 | 5,31E-05 |
|---|---|---|---|---|
| Base | 144,409 | 165,665 | 1306,461 | 2809,519 |
| 0.1 (ZnO) | 153,096 | 172,568 | 1398,979 | 2942,294 |
| 0.4 (ZnO) | 149,212 | 175,837 | 1385,969 | 3074,007 |
| 0.7 (ZnO) | 151,563 | 174,990 | 1319,291 | 3055,949 |
| 0.1 (MoS2) | 150,490 | 170,751 | 1372,236 | 3026,208 |
| 0.4 (MoS2) | 150,745 | 172,749 | 1408,918 | 3062,057 |
| 0.7 (MoS2) | 154,833 | 182,982 | 1441,263 | 3112,246 |

**Fig. 10.** Change of pumping power as a function of flow rate at different concentrations.

## 5. Conclusion

The effects of ZnO and $MoS_2$ NPs on the viscosity, tribological, and physicochemical attributes of diesel oil were evaluated. The following outcomes can be presented:

1. It was noticed that the kinematic viscosity and viscosity index of the samples raised with the incorporation of nanoparticles. Furthermore, the rise in kinematic viscosity grew by rising nanoparticle concentration. At each concentration of nanoparticles, ZnO nanofluids had higher kinematic viscosity compared to the $MoS_2$ nanofluids. The maximum rise in the kinematic viscosity was seen at 0.7 wt.% for each nanofluid. Walther equation

foretells well the kinematic viscosity−temperature relation. The selected theoretical models do not predict the relative viscosity enhancement with nanoparticle volume fraction.

2. Having fewer COF values and lower the roughness average of surfaces ($R_a$), it can be inferred that the ZnO and $MoS_2$ nanofluids had more desirable tribological characteristics. The optimal content of ZnO and $MoS_2$ NPs were 0.4 wt.% and 0.7 wt.%, respectively.
3. Evaluating the effect of the nanoparticles content on friction factor at the measured flow rates and inlet velocities showed that the friction factor increased by adding the NPs to the base fluid. In addition, the pumping power was enhanced by the incorporation of nanoparticles.

## 6. References


1. Choi, S.U. and J.A. Eastman, *Enhancing thermal conductivity of fluids with nanoparticles*. 1995, Argonne National Lab., IL (United States).
2. Zafarani-Moattar, M.T., et al., *Stability and rheological properties of nanofluids containing ZnO nanoparticles, poly (propylene glycol) and poly (vinyl pyrrolidone).* Fluid Phase Equilibria, 2015. **403**: p. 136-144.
3. Zeinali Heris, S., S.M. Nowee Baghban, and S.H. Noie Baghban, *Thermal behavior of a two phase closed thermosyphon using CuO/water nanofluid.* International Journal of Microscale and Nanoscale Thermal and Fluid Transport Phenomena, 2010. **1**.
4. Rashidi, S., et al., *Heat transfer coefficient prediction of metal oxides based water nanofluids under laminar flow regime using adaptive neuro-fuzzy inference system.* Journal of Dispersion Science and Technology, 2016. **37**.
5. Salimi-Yasar, H., S.Z. Heris, and M. Shanbedi, *Influence of soluble oil-based TiO2 nanofluid on heat transfer performance of cutting fluid.* Tribology International, 2017. **112**: p. 147-154.
6. Javadpour, R., S.Z. Heris, and Y. Mohammadfam, *Optimizing the effect of concentration and flow rate of water/MWCNTs nanofluid on the performance of a forced draft cross-flow cooling tower.* Energy, 2020. **217**: p. 119420.
7. Zahmatkesh, I., et al., *Effect of nanoparticle shape on the performance of thermal systems utilizing nanofluids: A critical review.* Journal of Molecular Liquids, 2020: p. 114430.
8. Kahani, M., et al., *Application of M5 tree regression, MARS, and artificial neural network methods to predict the Nusselt number and output temperature of CuO based nanofluid flows in a car radiator.* International Communications in Heat and Mass Transfer, 2020. **116**: p. 104667.
9. Mariano, A., et al., *Thermal conductivity, rheological behaviour and density of non-Newtonian ethylene glycol-based SnO2 nanofluids.* Fluid phase equilibria, 2013. **337**: p. 119-124.

10. Wang, B., et al., *Thermal conductivity and rheological properties of graphite/oil nanofluids.* Colloids and Surfaces A: Physicochemical and Engineering Aspects, 2012. **414**: p. 125-131.
11. Agarwal, S., V.K. Chhibber, and A.K. Bhatnagar, *Tribological behavior of diesel fuels and the effect of anti-wear additives.* Fuel, 2013. **106**: p. 21-29.
12. Salimi-Yasar, H., et al., *Experimental investigation of thermal properties of cutting fluid using soluble oil-based TiO2 nanofluid.* Powder Technology, 2017. **310**: p. 213-220.
13. Heris, Z. and Saeed, *Effect of TiO2 Nanoparticle on Rheological Behavior of Polyvinyl alcohol Solution.* Journal of Vinyl and Additive Technology, 2017. **32**.
14. Shakouri, A., et al., *Effect of TiO2 nanoparticle on rheological behavior of poly (vinyl alcohol) solution.* Journal of Vinyl and Additive Technology, 2017. **23**(3): p. 234-240.
15. Yu, L., et al., *Experimental investigation on rheological properties of water based nanofluids with low MWCNT concentrations.* International Journal of Heat and Mass Transfer, 2019. **135**: p. 175-185.
16. Izadkhah, M.-S. and S.Z. Heris, *Influence of Al 2 O 3 nanoparticles on the stability and viscosity of nanofluids.* Journal of Thermal Analysis and Calorimetry, 2019. **138**(1): p. 623-631.
17. Pourpasha, H., S.Z. Heris, and A. Asadi, *Experimental investigation of nano-TiO 2/turbine meter oil nanofluid.* Journal of Thermal Analysis and Calorimetry, 2019. **138**(1): p. 57-67.
18. Bhaumik, S., B.R. Mathew, and S. Datta, *Computational intelligence-based design of lubricant with vegetable oil blend and various nano friction modifiers.* Fuel, 2019. **241**: p. 733-743.
19. Pourpasha, H., et al., *The effect of multi-wall carbon nanotubes/turbine meter oil nanofluid concentration on the thermophysical properties of lubricants.* Powder Technology, 2020.
20. Singh, Y., et al., *Development of bio-based lubricant from modified desert date oil (balanites aegyptiaca) with copper nanoparticles addition and their tribological analysis.* Fuel, 2020. **259**: p. 116259.
21. Singh, Y., et al., *Chemical modification of juliflora oil with trimethylolpropane (TMP) and effect of TiO2 nanoparticles concentration during tribological investigation.* Fuel, 2020. **280**: p. 118704.
22. Singh, Y., et al., *Effect of SiC nanoparticles concentration on novel feedstock Moringa Oleifera chemically treated with neopentylglycol and their trobological behavior.* Fuel, 2020. **280**: p. 118630.
23. Zhang, Y., et al., *Tribological performance of CuS–ZnO nanocomposite film: The effect of CuS doping.* Tribology International, 2013. **58**: p. 7-11.
24. Imani-Mofrad, P., Z.H. Saeed, and M. Shanbedi, *Experimental investigation of filled bed effect on the thermal performance of a wet cooling tower by using ZnO/water nanofluid.* Energy Conversion and Management, 2016. **127**: p. 199-207.
25. Leitner, J., et al., *Thermodynamic properties of nanostructured ZnO.* Applied Materials Today, 2018. **10**: p. 1-11.
26. Lamba, N., et al., *ZnO catalyzed transesterification of Madhuca indica oil in supercritical methanol.* Fuel, 2019. **242**: p. 323-333.
27. Wang, L., et al., *The synergistic effect between ZnO and ZnCr2O4 on the catalytic performance for isobutanol synthesis from syngas.* Fuel, 2019. **253**: p. 1570-1577.

28. Mousavi, S.B. and S.Z. Heris, *Experimental investigation of ZnO nanoparticles effects on thermophysical and tribological properties of diesel oil.* International Journal of Hydrogen Energy, 2020. **45**(43): p. 23603-23614.
29. Singh, Y., et al., *Effect of ZnO nanoparticles concentration as additives to the epoxidized Euphorbia Lathyris oil and their tribological characterization.* Fuel, 2021. **285**: p. 119148.
30. Xie, H., et al., *Lubrication performance of MoS2 and SiO2 nanoparticles as lubricant additives in magnesium alloy-steel contacts.* Tribology International, 2016. **93**: p. 63-70.
31. Mousavi, S.B., S.Z. Heris, and M.G. Hosseini, *Experimental investigation of MoS2/diesel oil nanofluid thermophysical and rheological properties.* International Communications in Heat and Mass Transfer, 2019. **108**: p. 104298.
32. Padma, R., et al., *Structural, chemical, and electrical parameters of Au/MoS2/n-GaAs metal/2D/3D hybrid heterojunction.* Journal of colloid and interface science, 2019. **550**: p. 48-56.
33. Janbozorgi, M., et al., *Improving tribological behavior of friction stir processed A413/SiCp surface composite using MoS2 lubricant particles.* Transactions of Nonferrous Metals Society of China, 2017. **27**(2): p. 298-304.
34. Wu, H., et al., *An investigation on the lubrication mechanism of MoS2 nanoparticles in unidirectional and reciprocating sliding point contact: the flow pattern effect around contact area.* Tribology International, 2018. **122**: p. 38-45.
35. Gajrani, K.K., et al., *Thermal, rheological, wettability and hard machining performance of MoS2 and CaF2 based minimum quantity hybrid nano-green cutting fluids.* Journal of Materials Processing Technology, 2019. **266**: p. 125-139.
36. Dinesh, R., et al., *Investigation of tribological and thermophysical properties of engine oil containing nano additives.* Materials Today: Proceedings, 2016. **3**(1): p. 45-53.
37. Esfe, M.H., A.A.A. Arani, and S. Esfandeh, *Improving engine oil lubrication in light-duty vehicles by using of dispersing MWCNT and ZnO nanoparticles in 5W50 as viscosity index improvers (VII).* Applied Thermal Engineering, 2018. **143**: p. 493-506.
38. Alves, S., et al., *Tribological behavior of vegetable oil-based lubricants with nanoparticles of oxides in boundary lubrication conditions.* Tribology International, 2013. **65**: p. 28-36.
39. Cabaleiro, D., et al., *Thermal conductivity of dry anatase and rutile nano-powders and ethylene and propylene glycol-based TiO2 nanofluids.* The Journal of Chemical Thermodynamics, 2015. **83**: p. 67-76.
40. Battez, A.H., et al., *The tribological behaviour of ZnO nanoparticles as an additive to PAO6.* Wear, 2006. **261**(3-4): p. 256-263.
41. Moosavi, M., E.K. Goharshadi, and A. Youssefi, *Fabrication, characterization, and measurement of some physicochemical properties of ZnO nanofluids.* International journal of heat and fluid flow, 2010. **31**(4): p. 599-605.
42. Zeinali Heris, S., et al., *Rheological behavior of zinc-oxide nanolubricants.* Journal of Dispersion Science and Technology, 2015. **36**(8): p. 1073-1079.
43. Cabaleiro, D., et al., *Transport properties and heat transfer coefficients of ZnO/(ethylene glycol+ water) nanofluids.* International Journal of Heat and Mass Transfer, 2015. **89**: p. 433-443.

44. He, Y., et al., *Boiling heat transfer characteristics of ethylene glycol and water mixture based ZnO nanofluids in a cylindrical vessel.* International Journal of Heat and Mass Transfer, 2016. **98**: p. 611-615.
45. Pietruszka, R., et al., *Abrasion resistance of ZnO and ZnO: Al films on glass substrates by atomic layer deposition.* Surface and Coatings Technology, 2017. **319**: p. 164-169.
46. Nadooshan, A.A., H. Eshgarf, and M. Afrand, *Evaluating the effects of different parameters on rheological behavior of nanofluids: A comprehensive review.* Powder Technology, 2018. **338**: p. 342-353.
47. Hu, E., et al., *Tribological properties of 3 types of MoS 2 additives in different base greases.* Lubrication Science, 2017. **29**(8): p. 541-555.
48. Zawawi, N., et al., *Thermo-physical properties of Al2O3-SiO2/PAG composite nanolubricant for refrigeration system.* international journal of refrigeration, 2017. **80**: p. 1-10.
49. Zawawi, N., et al., *Experimental investigation on thermo-physical properties of metal oxide composite nanolubricants.* International Journal of Refrigeration, 2018. **89**: p. 11-21.
50. Coelho, M., et al., *Permittivity and electrical conductivity of copper oxide nanofluid (12 nm) in water at different temperatures.* The Journal of Chemical Thermodynamics, 2019. **132**: p. 164-173.
51. Ding, M., et al., *The excellent anti-wear and friction reduction properties of silica nanoparticles as ceramic water lubrication additives.* Ceramics International, 2018. **44**(12): p. 14901-14906.
52. Heris, S.Z., M.N. Esfahany, and S.G. Etemad, *Experimental investigation of convective heat transfer of Al2O3/water nanofluid in circular tube.* International journal of heat and fluid flow, 2007. **28**(2): p. 203-210.
53. Oh, D.-W., et al., *Thermal conductivity measurement and sedimentation detection of aluminum oxide nanofluids by using the 3ω method.* International Journal of Heat and Fluid Flow, 2008. **29**(5): p. 1456-1461.
54. Abu-Nada, E., *Effects of variable viscosity and thermal conductivity of Al2O3–water nanofluid on heat transfer enhancement in natural convection.* International Journal of Heat and Fluid Flow, 2009. **30**(4): p. 679-690.
55. Noie, S.H., et al., *Heat transfer enhancement using Al2O3/water nanofluid in a two-phase closed thermosyphon.* International Journal of Heat and Fluid Flow, 2009. **30**(4): p. 700-705.
56. Heris, S.Z., et al., *Laminar convective heat transfer of Al2O3/water nanofluid through square cross-sectional duct.* International Journal of Heat and Fluid Flow, 2013. **44**: p. 375-382.
57. Karimi, A., et al., *Experimental investigation on thermal conductivity of water based nickel ferrite nanofluids.* Advanced Powder Technology, 2015. **26**(6): p. 1529-1536.
58. Minea, A.-A. and W.M. El-Maghlany, *Natural convection heat transfer utilizing ionic nanofluids with temperature-dependent thermophysical properties.* Chemical Engineering Science, 2017. **174**: p. 13-24.
59. Cao, Z., Y. Xia, and X. Xi, *Nano-montmorillonite-doped lubricating grease exhibiting excellent insulating and tribological properties.* Friction, 2017. **5**(2): p. 219-230.
60. Luo, T., et al., *Tribological properties of Al2O3 nanoparticles as lubricating oil additives.* Ceramics International, 2014. **40**(5): p. 7143-7149.

61. Noroozi, N., D. Grecov, and S. Shafiei-Sabet, *Estimation of viscosity coefficients and rheological functions of nanocrystalline cellulose aqueous suspensions.* Liquid Crystals, 2014. **41**(1): p. 56-66.
62. Elemsimit, H.A. and D. Grecov, *Impact of liquid crystal additives on a canola oil-based bio-lubricant.* Proceedings of the Institution of Mechanical Engineers, Part J: Journal of Engineering Tribology, 2015. **229**(2): p. 126-135.
63. Shariatzadeh, M.J. and D. Grecov, *Cellulose Nanocrystals Suspensions as Water-Based Lubricants for Slurry Pump Gland Seals.* International Journal of Aerospace and Mechanical Engineering, 2018. **12**(6): p. 603-607.
64. Shariatzadeh, M., *Cellulose nanocrystals aqueous suspensions as water-based lubricants*. 2018, University of British Columbia.
65. Shariatzadeh, M. and D. Grecov, *Aqueous suspensions of cellulose nanocrystals as water-based lubricants.* Cellulose, 2019. **26**(7): p. 4665-4677.
66. Zakani, B. and D. Grecov, *Yield stress analysis of cellulose nanocrystalline gels.* Cellulose, 2020. **27**(16): p. 9337-9353.
67. Wu, P.-R., et al., *An investigation on tribological properties of the chemically capped zinc borate (ZB)/MoS2 nanocomposites in oil.* Journal of industrial and engineering chemistry, 2018. **63**: p. 157-167.
68. Sanukrishna, S. and M.J. Prakash, *Experimental studies on thermal and rheological behaviour of TiO2-PAG nanolubricant for refrigeration system.* International Journal of Refrigeration, 2018. **86**: p. 356-372.
69. Sharif, M., et al., *Investigation of thermal conductivity and viscosity of Al2O3/PAG nanolubricant for application in automotive air conditioning system.* international journal of refrigeration, 2016. **70**: p. 93-102.
70. Khairul, M., et al., *Effects of surfactant on stability and thermo-physical properties of metal oxide nanofluids.* International Journal of Heat and Mass Transfer, 2016. **98**: p. 778-787.
71. Jabbari, F., A. Rajabpour, and S. Saedodin, *Thermal conductivity and viscosity of nanofluids: a review of recent molecular dynamics studies.* Chemical Engineering Science, 2017. **174**: p. 67-81.
72. Mousavi, S.B., S.Z. Heris, and P. Estellé, *Experimental comparison between ZnO and MoS 2 nanoparticles as additives on performance of diesel oil-based nano lubricant.* Scientific Reports, 2020. **10**(1): p. 1-17.
73. Esfe, M.H., et al., *Viscosity and rheological properties of antifreeze based nanofluid containing hybrid nano-powders of MWCNTs and TiO2 under different temperature conditions.* Powder technology, 2019. **342**: p. 808-816.
74. Chen, N.H., *An explicit equation for friction factor in pipe.* Industrial & Engineering Chemistry Fundamentals, 1979. **18**(3): p. 296-297.
75. McKeon, B., et al., *Friction factors for smooth pipe flow.* Journal of Fluid Mechanics, 2004. **511**: p. 41-44.
76. White, F.M., *Fluid mechanics*. 2011, McGraw-Hill: New York.
77. Peiyi, W. and W. Little, *Measurement of friction factors for the flow of gases in very fine channels used for microminiature Joule-Thomson refrigerators.* Cryogenics, 1983. **23**(5): p. 273-277.
78. Holman, J.P., *Experimental methods for engineers*. 2001.

79. Chen, C., P. Liu, and C. Lu, *Synthesis and characterization of nano-sized ZnO powders by direct precipitation method.* Chemical Engineering Journal, 2008. **144**(3): p. 509-513.
80. Wu, P.-R., et al., *Fabrication and tribological properties of oil-soluble MoS2 nanosheets decorated by oleic diethanolamide borate.* Journal of Alloys and Compounds, 2019. **770**: p. 441-450.
81. McCoull, N. and C. Walther, *Viscosity-temperature chart.* Lubrication, June, 1921. **7**: p. 1-16.
82. Einstein, A., *Investigations on the Theory of the Brownian Movement*. 1956: Courier Corporation.
83. Kole, M. and T. Dey, *Effect of aggregation on the viscosity of copper oxide–gear oil nanofluids.* International Journal of Thermal Sciences, 2011. **50**(9): p. 1741-1747.
84. Kole, M. and T. Dey, *Role of interfacial layer and clustering on the effective thermal conductivity of CuO–gear oil nanofluids.* Experimental Thermal and Fluid Science, 2011. **35**(7): p. 1490-1495.
85. Rashin, M.N. and J. Hemalatha, *Viscosity studies on novel copper oxide–coconut oil nanofluid.* Experimental Thermal and Fluid Science, 2013. **48**: p. 67-72.
86. Kotia, A., et al., *Effect of copper oxide nanoparticles on thermophysical properties of hydraulic oil-based nanolubricants.* Journal of the Brazilian Society of Mechanical Sciences and Engineering, 2017. **39**(1): p. 259-266.
87. Corcione, M., *Empirical correlating equations for predicting the effective thermal conductivity and dynamic viscosity of nanofluids.* Energy conversion and management, 2011. **52**(1): p. 789-793.
88. Sharma, K., et al., *Correlations to predict friction and forced convection heat transfer coefficients of water based nanofluids for turbulent flow in a tube.* International Journal of Microscale and Nanoscale Thermal and Fluid Transport Phenomena, 2012. **3**(4): p. 1-25.
89. Mosarof, M., et al., *Assessment of friction and wear characteristics of Calophyllum inophyllum and palm biodiesel.* Industrial Crops and Products, 2016. **83**: p. 470-483.
90. Ripoll, M.R., et al., *In situ tribochemical sulfurization of molybdenum oxide nanotubes.* Nanoscale, 2018. **10**(7): p. 3281-3290.
91. Cheah, M.Y., et al., *Physicochemical and tribological properties of microalgae oil as biolubricant for hydrogen-powered engine.* International Journal of Hydrogen Energy, 2019.
92. Naddaf, A., S.Z. Heris, and B. Pouladi, *An experimental study on heat transfer performance and pressure drop of nanofluids using graphene and multi-walled carbon nanotubes based on diesel oil.* Powder Technology, 2019. **352**: p. 369-380.